Methylphosphonic Acid Oxidation Kinetics in Supercritical Water

Patricia A Sullivan and Jefferson W. Tester
Dept. of Chemical Engineering and Laboratory for Energy and the Environment, Massachusetts Institute of Technology, Cambridge, MA 02139

Oxidation and hydrolysis rates of the model organophosphorus compound, methylphosphonic acid (MPA), were measured in supercritical water. The effects of MPA concentration (0.5 to 1.0 mM), oxygen concentration (1.0 to 3.8 mM), temperature (478 to 572°C) and pressure (138 to 277 bar) on oxidation rates were determined for residence times ranging from 3.0 to 9.5 s. The MPA oxidation rate was dependent on both oxygen concentration and pressure (or water density), but was relatively independent of initial MPA concentration. The only phosphorus-containing product was phosphoric acid, while the primary carbon-containing products included carbon monoxide, methane, and carbon dioxide. Data were regressed to an empirical global rate law with a pre-exponential factor of $10^{14.0\pm1.6}$ (s^{-1} $M^{-1.47}$), an activation energy of 228±22 kJ/mol, a first-order MPA dependence, an oxygen order of 0.30±0.18, and a water order of 1.17±0.30 (all parameters to 95% confidence). A macroscopic model was also developed to estimate reaction rate constants and oxygen dependences of the major identified reaction pathways. © 2004 American Institute of Chemical Engineers *AIChE J,* 50: 673–683, 2004
Keywords: reaction kinetics, supercritical water, oxidation, reaction pathways, organophosphorous

Introduction

Supercritical water is an excellent solvent for the oxidation of organic compounds due to the high solubility of both organics and oxygen in water above its critical point (T_c=374°C, P_c=221 bar), thus avoiding interphase mass transfer limitations. At supercritical operating conditions (T >475°C, P >240 bar), oxidation proceeds quickly and completely for most H-C-N compounds with water, carbon dioxide, and molecular nitrogen as the main products. For compounds containing heteroatoms such as chlorine, sulfur, and phosphorus, oxidation also produces the corresponding inorganic acids: HCl, H_2SO_4, and H_3PO_4, which can be neutralized to their corresponding salts and separated as a concentrated liquid brine or precipitated solid. Supercritical water oxidation (SCWO) has most often been used to treat dilute organic waste streams that can be otherwise difficult to remediate. The SCWO process can effectively treat a wide range of toxic aqueous waste streams to acceptable destruction and removal efficiency (DRE) levels, which are often greater than 99.99%. Additional information on SCWO technology is available in the reviews by Modell (1989), Tester et al. (1993), Gloyna and Li (1995), Savage et al. (1995), Tester and Cline (1999), Savage (1999), Shaw and Dahmen (2000), and Kritzer and Dinjus (2001).

The U.S. Army currently employs SCWO as an alternative secondary treatment method to destroy stockpiled chemical agents. Typically, the first stage is neutralization with a caustic aqueous solution which can achieve a DRE >99.9999%, the lower destruction limit for all toxic compounds. Nonetheless, the neutralization step leaves chemical agent precursors in the effluent that must be treated by a secondary method (NRC, 2000). SCWO is an attractive treatment choice because oxidation is carried out in a closed, controlled system that can be easily shut down should problems arise. Also, operating temperatures are much lower than those of incineration, so nitrogen oxides do not form (Shaw and Dahmen, 2000).

Correspondence concerning this article should be addressed to J. W. Tester at testerel@mit.edu.

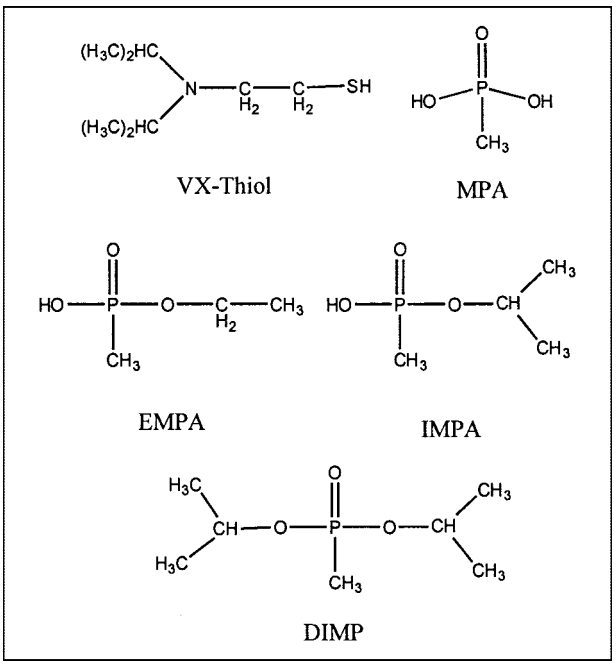

Figure 1. Organophosphorus chemical agent hydrolysis products.

One of the largest class of chemical warfare agents is that of organophosphorus nerve agents, which include VX, Sarin, and Soman. The caustic hydrolysis products of VX are ethylmethylphosphonic acid (EMPA), methylphosphonic acid (MPA), and diisopropylaminoethanethiol (VX-thiol), while those for Sarin include isopropylmethylphosphonic acid (IMPA), MPA, and di-isopropylmethylphosphonate (DIMP), as shown in Figure 1 (ACWA, 1999). These caustic hydrolysis products can be oxidized in an SCW reactor to the final oxidation products of H_3PO_4, H_2SO_4, CO_2, and H_2O. However, aside from the high DREs reported for oxidation of the hydrolysis products, minimal data are available for SCWO processing of phosphonates at intermediate conversions. In particular, quantitative characterization of oxidation kinetics and reaction pathways under different operating conditions is very limited.

The present study examines the SCWO kinetics of the model compound, MPA ($PO(OH)_2CH_3$) because it is a key, refractory intermediate in the oxidation of organophosphorus agents. Quantitative information regarding MPA oxidation kinetics in SCW is pertinent for SCWO process design and optimization. Other organophosphorus simulants, such as dimethylmethylphosphonate (DMMP), diethylmethylphosphonate (DEMP), and DIMP, are commonly used as model compounds in atmospheric combustion studies to explore organophosphorus pyrolysis and oxidation kinetics under incineration conditions at low pressures (Zegers and Fisher, 1996, 1998; Werner and Cool, 1998; Korobeinichev et al., 2000). However, in sub- and supercritical water, DMMP hydrolyzes quickly to MPA (Turner, 1993). MPA is an ideal model compound to study due to its refractory nature in SCW and its importance in a number of organophosphorus oxidation mechanisms.

Since MPA only retains a single methyl group from the original agent, knowledge of its oxidation kinetics permits a focused study of the phosphorus-carbon (P–C) bond in the phosphonate structure. The P–C bond is inert to acidic and basic hydrolysis with bond cleavage occuring primarily through radical mediated pathways (Cordeiro et al., 1986; Schowanek and Verstraete, 1991). Several organophosphorus combustion mechanisms for DMMP have proposed P-C bond cleavage reactions; however, given the multiple sources of carbon in DMMP, it was difficult for the authors to correctly infer the actual elementary reactions from the measured intermediate concentration profiles (Werner and Cool, 1998; Korobeinichev et al., 2000; Glaude et al., 2000). Insight into possible radical pathways for P–C bond cleavage can be obtained from the knowledge of MPA oxidation rates and carbon yields under well-defined experimental conditions.

There have been two previous experimental studies of organophosphorus oxidation kinetics in SCW (Turner, 1993; Bianchetta et al., 1999). Turner (1993) reported that DMMP hydrolyzed quickly and completely to MPA and methanol at temperatures of 300 to 520°C, a pressure of 276 bar, and residence times of 7 to 57 s in the preheater section of a tubular reactor system. In essence, Turner's experiments measured the co-oxidation kinetics of a mixed MPA and methanol feed stream. Due to the low temperature range studied, MPA conversions were generally less than 50%. A global rate law for MPA and methanol co-oxidation regressed from Turner's data yielded first-order behavior with respect to both MPA and oxygen concentrations.

More recently, Bianchetta et al.'s (1999) MPA SCWO study focused on measuring rates at high conversion, with over half of the experiments at conversions greater than 90% to represent more practical treatment applications. The experiments in this study were conducted at temperatures between 400 and 594°C, residence times between 3 and 83 s, a pressure of 276 bar, and oxygen concentrations at 110 to 200% of stoichiometric amounts. At 550°C, 276 bar, and 200% stoichiometric oxygen, conversions of greater than 99% were measured at residence times less than 20 s. Reaction pathways were inferred from the analysis of carbon-containing intermediates and products, and a global rate law was regressed from the experimental data. First-order rate constants were also estimated for the major reaction pathways.

The primary goal of our work was to characterize the oxidation kinetics of MPA in SCW at moderate conversions where derived kinetic parameters are less uncertain and yield more quantitative insight into the MPA oxidation mechanism. We systematically explored the effects of temperature, residence time, oxygen concentration, MPA concentration, and pressure (or water density) on MPA conversion and on its product distribution at the conditions shown in Table 1. With higher quality data, a global rate expression could be regressed with

Table 1. Experimental Variables and Ranges Studied in This Study

Experimental Variable	Range
Temperature, T	478–572°C
Residence time, τ	3.0–9.5 s
Initial MPA Concentration $[MPA]_0$	0.5–1.0 mM
Fuel Equivalence Ratio, Φ	0.55–1.97
Pressure, P	138–277 bar
Water Density, ρ	0.041–0.095 g/mL

the dependence on MPA, oxygen, and water concentrations determined with significantly lower uncertainty. In addition, macroscopic reaction rates for major pathways could be accurately estimated to determine the relative reaction rates in the MPA oxidation system.

Experimental section

All experiments were conducted in the plug flow reactor system that has been used previously in our laboratory (DiNaro et al., 2000a; Phenix et al., 2002). As DiNaro (1999) provides a detailed description of the experimental apparatus, only a brief description is provided below.

The organic and oxidant feedstreams were fed separately to the reactor using two independently controlled, digital HPLC pumps (Rainin, SD-200). The organic feed was prepared by making an aqueous solution of MPA (98 wt. %, Aldrich Chemical Company) used as received and dissolved in deionized water. Hydrogen peroxide (H_2O_2) was used as the oxidant source for these experiments. H_2O_2 decomposes completely to oxygen and water when heated in the preheater section before the reactor inlet as verified by previous experiments (Phenix et al., 2002). The H_2O_2 feed solution was prepared by diluting a 30 wt. % solution of ACS grade H_2O_2 (Aldrich Chemical Company) with deionized water to the desired concentration. Both feed solutions were degassed using helium gas to ensure the removal of oxygen. Following degassing, the HPLC pumps pressurized the feed streams and delivered them to the reactor system.

The organic and oxidant feedstreams were preheated to reactor temperature by different methods before reaching the reactor. The first stage employed direct ohmic heating (DOH) which heated the streams to a reaction temperature using electric resistive heating by applying a voltage across 9.5-m lengths of 1/16 in. (1.6 mm) O.D. x 0.01 in. (0.25 mm) wall Hastelloy (HC-276) tubing. The temperature regulation of the DOH system was accomplished by controlling the applied voltage levels with two separate PID controllers (Omega, p/n CN9000A) whose 1/32 in. (0.8 mm) type K thermocouples were located directly after the DOH preheater section. The last 0.5 m of the 9.5 m DOH preheating coils located outside of the insulated DOH housing were also traced with heat tape to prevent heat losses. The second stage maintained the temperature in the preheater tubing between the DOH system and the reactor inlet. In the 30-cm section between the DOH thermocouples and the reactor sandbath, resistive cable heaters (Watlow, p/n 62H24A6X, 1/16 in. (1.6 mm) O.D. x 2 ft. (61 cm) long, 10 V, 240 W max.) were wrapped around the tubing with their power controlled by variable transformers to minimize heat losses. Once the organic and oxidant streams entered the fluidized sandbath, each stream passed through an additional 5.2 m coiled length of 1/16 in. (1.6 mm) O.D. x 0.01 in. (0.25 mm) wall HC-276 preheater tubing to ensure isothermality at the reactor inlet.

Mixing of the organic and the oxidant streams occured in a specially modified 1/8 in. (3.2 mm) HC-276 cross from High Pressure Equipment (p/n 60-24HF2). The feedstreams entered the cross in a side-entry configuration at an angle of 90° from each other. The internal diameters of the two arms through which the feedstreams entered the cross were reduced from their original 1/16 in. (1.6 mm) I.D. to 0.01 in. (0.25 mm) I.D. by press fitting short lengths of 1/16 in. (1.6 mm) O.D. x 0.01 in. (0.25 mm) I.D. 316 SS (stainless steel) tubing into those arms. This modification was performed to increase the velocities of the organic and oxidant feeds, and thus increase the rate of mixing. Details of the mixing cross configuration are found in Phenix et al. (2002). A 1/16 in. Type K thermocouple was seated in a side port of the cross, and its tip extended into the fluid to ensure that the measured temperature was that of the fluid. The fourth port of the cross was connected to the reactor inlet where the reactor was a 1/4 in. (6.36 mm) O.D. x 0.067 in. (1.7 mm) I.D. coiled length of Inconel 625 tubing with an internal volume of 10.71 ± 0.60 cm^3. A second 1/16 in. Type K thermocouple was seated in an 1/8 in. (3.2 mm) HC-276 tee at the reactor exit. A 26 cm length of 1/4 in. (6.35 mm) O.D. x 1/16 in. (1.6 mm) I.D. insulated HC-276 tubing rose out of the sandbath and connected the reactor to the heat exchanger. Temperatures were monitored continuously with HOTMUX software by seven different thermocouples located in the preheater, reactor, sandbath, and heat exchanger sections.

After exiting the reactor, the effluent entered the inner tube of a shell-and-tube heat exchanger and was immediately quenched. The system pressure was controlled by a spring-loaded, manual backpressure regulator (Tescom, p/n 26-3200). Once the fluid exited the regulator, it flashed to atmospheric pressure and the two-phase mixture was separated into two streams by the gas-liquid separator. The gas flow rate was measured using a soap bubble flowmeter and a stopwatch, while liquid flow rates were measured using a 50-mL Class A volumetric flask and a stopwatch. Gas samples were withdrawn using a gas-tight syringe from the sampling port and were subsequently analyzed on gas chromatographs. Liquid samples were removed from the liquid effluent and injected onto an ion chromatograph.

For each experimental run, the reactor was stabilized for at least an hour at each set of operating conditions to ensure steady-state operation. Measurements were then taken over the course of another hour where at least six liquid and four gas samples were drawn and at least six liquid and gas-flow rates were recorded. The inlet MPA feed concentration was measured from at least four samples, two taken at the beginning and at the end of the set of runs, to ensure that the feed concentration remained constant. The H_2O_2 feed concentration was also sampled from the oxidant feed vessel at the beginning and end of the set of runs. The H_2O_2 feed concentrations were measured by a ceric ion titration method to determine the oxygen concentration at the reactor inlet.

All liquid samples were subjected to multiple analytical determinations of composition using an ion chromatograph to measure MPA and phosphoric acid concentrations in the feed and effluent. The ion chromatograph was equipped with a Dionex IonPac AS11 anion column, a Dionex IonPac AG11 guard column, a Rainin HPXL pump, a Dionex Anion Self-Regenerating Suppressor ASRS-I, a Dionex DS3 Detection Stabilizer, and a Dionex ED40 electrochemical detector operated in conductivity mode with a 21 mM NaOH eluent.

To analyze the gas effluent, three separate gas chromatographs were employed. For the light gases, such as oxygen, nitrogen, carbon monoxide, and carbon dioxide, an HP 5890 Series II GC was used with a thermal conductivity detector (TCD), and helium as the carrier gas. To ensure complete separation of the gases, two columns were connected in series

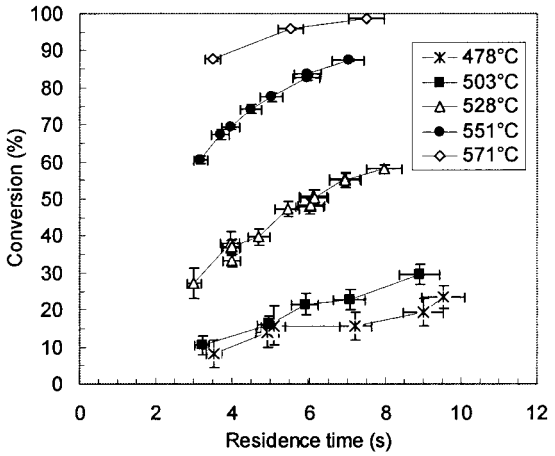

Figure 2. MPA conversion as a function of temperature and residence time at stoichiometric conditions (Φ = 0.98 ± 0.07), $[MPA]_0$ = 0.99 ± 0.03 mM, and P = 246 ± 1 bar.

with an air actuated switching valve. The first column was a 5 ft (1.5 m) x 1/8 in. (3.2 mm) 60/80 mesh Carboxen 1000 column which separates the carbon containing gases and connects to an 8 ft (2.4 m) x 1/8 in. (3.2 mm) 60/80 mesh Molsieve 5Å column which separates the O_2 and N_2. A second HP 5890 Series II with a TCD detector employed nitrogen as the carrier gas to analyze for helium and hydrogen. This GC also used the 60/80 mesh Carboxen 1000 and 60/80 mesh Molsieve 5Å for separation. A third HP 5890 Series II GC with an FID detector used a helium carrier gas to analyze for light hydrocarbons, such as methane. The column was a bonded Astec PLOT column that can separate hydrocarbons up to C-10.

Results and Discussion

A total of 4 hydrolysis and 67 oxidation experiments were conducted at varying temperatures (T), residence times (τ), fuel equivalence ratios (Φ), pressures (P) or water densities (ρ), and initial MPA concentrations ($[MPA]_0$) (see Table 1). The fuel equivalence ratio is defined as

$$\Phi \equiv \frac{([MPA]/[O_2])_0}{([MPA]/[O_2])_{stoichiometric}} \quad (1)$$

where the stoichiometric ratio for MPA:O_2 is 1:2 for complete conversion of MPA to H_3PO_4, CO_2, and H_2O. As defined, a value of $\Phi>1$ denotes oxygen-lean conditions and $\Phi<1$ denotes oxygen-rich conditions. The bulk of the data were taken at stoichiometric conditions ($\Phi=1$), $P=246$ bar, and $[MPA]_0=1$ mM in an effort to be consistent with previous experiments in our laboratory.

Carbon and phosphorus balances were calculated for all experiments based on measured inlet MPA concentrations and measured outlet product and MPA concentrations. For the phosphorus balance, phosphoric acid was the only detected phosphorus-containing product and the average phosphorus balance was 101±3% at a 99% confidence interval with a range from 95 to 104%. The detectable carbon-containing products and intermediates were carbon monoxide, methane, and carbon dioxide, all measured in the gas phase. The carbon balances had an average value of 103±3% with a range of 94 to 109%. The larger range of the carbon balances can most likely be attributed to higher uncertainty in the gas phase measurements of these compounds.

For the uncertainty calculations, all confidence intervals were calculated by estimating that the uncertainty of all measured variables (temperature, liquid flow rate, gas-flow rate, analytical signals, and pressure) could be represented by a student's t-distribution from multiple measurements (usually greater than 6 measurements). The uncertainty was then propagated for all calculated values, such as conversion or reactor concentrations, using the differential method and reported at a 99% confidence interval. A table containing all of the experimental data is available in Sullivan (2003).

MPA hydrolysis

To determine the level of hydrolysis that occurred in the preheater and the reactor, a set of experiments was performed at $\tau=7$ s for temperatures between 503 and 571°C in the absence of any added oxygen (or H_2O_2). Experimental conversions varied between 3 and 6% with average errors of 3%, in agreement with the earlier study by Bianchetta et al. (1999). As a consequence, any conversion due to hydrolysis was ignored during the analysis of MPA oxidation results.

MPA oxidation

The effects of temperature and residence time on MPA oxidation rates were determined by a set of 36 experiments at $\Phi=0.98\pm0.07$, $P=246\pm1$ bar, and $[MPA]_0=0.99\pm0.03$ mM (see Table 1). As seen in Figure 2, MPA conversion is fairly low ($X<30\%$ at $\tau=8.9$ s) at $T\leq$ 503°C and conversion is almost complete ($X>99\%$) at $\tau=7.5$ s and $T=571$°C. To gain more insight into the MPA oxidation mechanism, conditions favoring moderate conversions were sought to better quantify the effects of operating variables on MPA oxidation. Given this

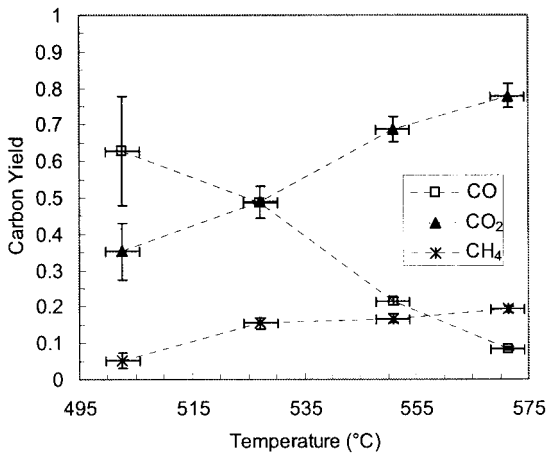

Figure 3. Species carbon yields for the carbon-containing intermediates, CO and CH_4, and product, CO_2, as a function of temperature at a constant residence time of 5.8 ± 0.4 s.

These data were taken at stoichiometric conditions (Φ = 0.97 ± 0.07), $[MPA]_0$ = 0.99 ± 0.03 mM, and P = 246 ± 1 bar.

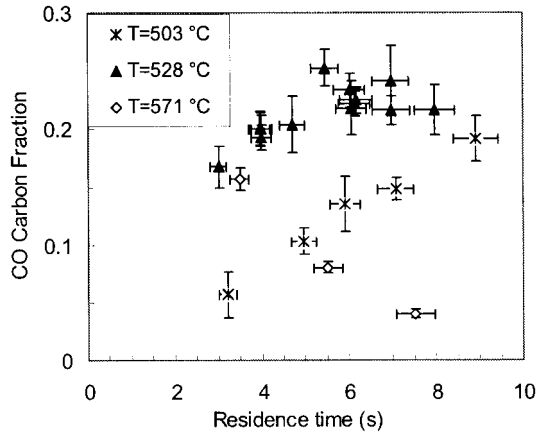

Figure 4. CO carbon fraction as a function of residence time and temperature at stoichiometric conditions (Φ = 0.98 ± 0.07), $[MPA]_0$ = 0.99 ± 0.03 mM, and P = 246 ± 1 bar.

goal, Φ and pressure variation experiments were conducted at T=528 and 551 °C where MPA conversions range between 25 and 85%.

The carbon yields of the intermediates, CH_4 and CO, and the final carbon containing product, CO_2, are plotted in Figure 3 as a function of temperature at τ=5.8±0.4 s. The carbon yield for species (i) is defined as

$$\text{Species } (i) \text{ carbon yield} \equiv \frac{\text{Moles of carbon in product } (i)}{\text{Total moles of carbon reacted}} \equiv \frac{[C_{\text{product}}]}{[\text{MPA}]_0 - [\text{MPA}]} \quad (2)$$

The yields of all carbon containing products and intermediates should sum to unity assuming mass balance closure. CO and CO_2 are the major MPA oxidation products, while CH_4 is a minor product whose yield is always less than 20% at these experimental conditions. In this temperature range, CO is a reactive intermediate whose yield decreases as temperature increases, while CH_4 is a refractory intermediate, as its yield increases with temperature. The CO_2 yield increased continually over the studied temperature range to a maximum value of almost 0.8 at T=571 °C where MPA conversion is 96%.

Since CO is a reactive intermediate in MPA oxidation, MPA and CO oxidation occur on similar reaction time scales. Two previous carbon monoxide oxidation studies have been conducted in our research group (Helling and Tester, 1987; Holgate et al., 1992; Holgate and Tester, 1994a) at similar conditions to the present MPA study (T=420 to 571 °C, τ=3.4 to 12.1 s, P=118 to 263 bar). CO oxidation rates are comparable to MPA's at these conditions; CO conversion is low (X<30%) at T=530°C and τ=5.5 s and high conversions (>90%) occur at T>560°C and τ=7 s. The relationship between MPA and CO oxidation rates can be seen by examining the CO carbon fraction, defined below, at different temperatures and residence times in Figure 4

$$\text{Species } (i) \text{ carbon fraction} \equiv \frac{\text{Moles of carbon in product } (i)}{\text{Total moles of carbon fed}} \equiv \frac{[C_{\text{product}}]}{[\text{MPA}]_0} \quad (3)$$

At T=503 °C, the CO carbon fraction is relatively low because MPA conversion is low, and it increases with residence time because CO is refractory at this temperature. The CO carbon fraction reaches a maximum at T=528°C where MPA conversion is substantial enough to produce a significant amount of CO, but CO oxidation is not yet fast enough to react completely. However, once the temperature reaches 571 °C, CO oxidation proceeds rapidly as evidenced by its decreasing fraction with residence time.

The other carbon-containing intermediate, methane, has also been previously studied at SCWO conditions (Webley and Tester, 1991; Savage et al., 1998). As compared to the CO intermediate, CH_4 is refractory at the lower temperature range of the present MPA study. As shown in Figure 3, the carbon yield of CH_4 increases from 0.05 at 503°C to 0.19 at 571°C. Based on previous CH_4 oxidation studies, temperatures greater than 600 °C would be required to achieve appreciable CH_4 conversion (>40%) at a residence time of 6 s. Thus, at the lower temperatures of the present study with slower CH_4 oxidation rates, CH_4 accumulation is expected.

Due to the existence of the two intermediates, CO and CH_4, Bianchetta et al. (1999) hypothesized that two separate pathways for MPA oxidation could exist: a primary reaction pathway through CO (k_1) and a minor pathway through CH_4 (k_2), as illustrated in Figure 5. Both of these pathways also form H_3PO_4 since it is the only phosphorus-containing product. Once formed, CH_4 reacts to CO (k_4) and CO is further oxidized to CO_2 (k_3). Because CO is an intermediate in CH_4 oxidation, one could also postulate a different mechanism where MPA reacts by a single pathway from CH_4 to CO and then to CO_2. However, because the reaction rate of CH_4 is not expected to be significant at these temperatures and residence times, the measured concentrations of CO and CO_2 cannot result primarily from CH_4 oxidation and this two pathway mechanism is more plausible.

The two-pathway macroscopic mechanism in Figure 5 presents a global view for P-C bond cleavage in this system. In an

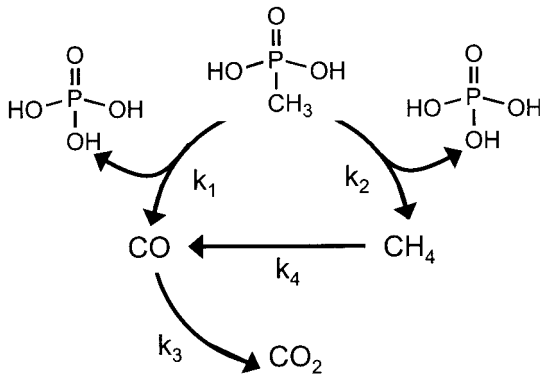

Figure 5. Macroscopic reaction pathway of the fate of carbon and phosphorus in the MPA oxidation system balancing in carbon and phosphorus only.

Note that water and oxygen provide a source for the oxygen and hydrogen necessary to balance stoichiometry. The MPA pathways to form carbon monoxide and methane (k_1 and k_2, respectively); both form phosphoric acid as the phosphorus-containing product. Subsequently, CH_4 oxidizes to CO (k_4) and CO reacts with oxygen to form CO_2 (k_3).

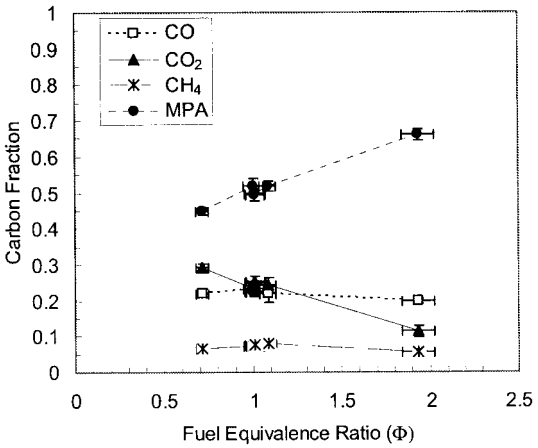

Figure 6. Species carbon fractions as a function of fuel equivalence ratio at T = 528 ± 3°C, τ = 6.0 ± 0.4 s, $[MPA]_0$ = 1.00 ± 0.03 mM, and P = 246 ± 1 bar.

(Note: $\Phi < 1$ denotes oxygen-rich conditions and $\Phi > 1$ denotes oxygen-lean conditions).

analysis of low pressure combustion mechanisms, only one MPA bimolecular reaction rate has been estimated (Korobeinichev et al., 2000; Glaude et al., 2000)

$$PO(OH)_2CH_3 + OH \leftrightarrow PO(OH)_3 + CH_3 \qquad (R1)$$

In this reaction, an OH radical adds to the phosphorus center and displaces a CH_3 radical from MPA. This single reaction could possibly account for the two MPA global pathways if the CH_3 reacted by two separate pathways to form CO and CH_4. However, a preliminary elementary reaction rate model indicates that in SCW at these conditions, the methyl radical primarily reacts with water to form methane with little formation of CO or CO_2, contrary to our experimental results. Given these results, additional P-C bond cleavage pathways for MPA oxidation appear to exist, as is discussed in more detail in a subsequent article that presents an elementary reaction rate model of MPA oxidation in supercritical water (Sullivan et al., 2004).

Dependence on fuel equivalence ratio

To explore the effect of oxygen on MPA conversion and carbon fraction, the fuel equivalence ratio was varied from sub to superstoichiometric values at temperatures of 503, 528, and 551°C with P=246±1 bar, and $[MPA]_0$=1.00±0.03 mM for a set of 13 experiments. The effect of Φ on carbon fraction at T=528±3 °C and τ=6.0±0.4 s is plotted in Figure 6 where Φ=0.67 is at 50% oxygen excess and Φ=2.0 is at 50% of stoichiometric oxygen. As Φ decreases or $[O_2]$ increases, MPA carbon fraction decreases implying that oxygen has a significant role in the formation of radicals in MPA oxidation at SCW conditions.

Carbon dioxide is the only carbon-containing product that was significantly affected by varying Φ at these conditions. The CO_2 carbon fraction increased as Φ decreased, while CO and CH_4 were generally unaffected by a change in Φ. Similar results were also obtained for the 551°C data. The CH_4 carbon fraction's lack of dependence on Φ suggests a nonoxidative formation route for methane from the methyl group of MPA. The oxidation rate of CO to CO_2 has an oxygen dependence to the order of 0.3 from previous studies (Holgate et al., 1992; Holgate and Tester, 1994a). Thus, the CO carbon fraction remaining approximately constant as Φ is varied indicates that the rates of CO formation, $k_1[MPA][O_2]^{b1}$, and CO destruction, $k_3[CO][O_2]^{b3}$, are approximately in balance and their ratio is essentially independent of oxygen at this residence time. It is somewhat surprising that these reaction rates would exhibit similar oxygen dependence since these macroscopic pathways occur through a series of elementary, radical reactions. Further insight into the relationship between the rates of CO formation and destruction is developed later.

Dependence on pressure/water density

Previous experimental studies have found that some organic compounds can exhibit a dependence on water density (DiNaro et al., 2000a; Holgate and Tester, 1994a; Koo et al., 1997). Unfortunately, at SCW conditions, the effects of pressure and water density are not easily separated since water density is a function of both pressure and temperature. Also, water's role as a solvent and/or a reactant in SCWO is not very well understood. Koo et al. (1997) attempted to decouple the effects of pressure and water density by adding helium, an inert gas, to adjust the system pressure while keeping the water density constant. They demonstrated that a reported increase in phenol conversion was due to an increase in water density. Additionally, analysis of elementary reaction rate models for SCWO indicates that the increase in water density or concentration, rather than the pressure, most likely caused the increase in conversion found experimentally for CO and benzene (Holgate and Tester, 1994b; DiNaro et al., 2000b).

For the present set of experiments, pressures were varied from a subcritical pressure of 138 bar to a supercritical pressure of 277 bar at T=528 and 551°C, Φ=1.01±0.05 and $[MPA]_0$=1.00±0.03 mM for a set of 15 experiments. As shown in Figure 7, MPA conversion approximately doubled over the water density range of 41 to 94 kg/m^3 at T=528°C.

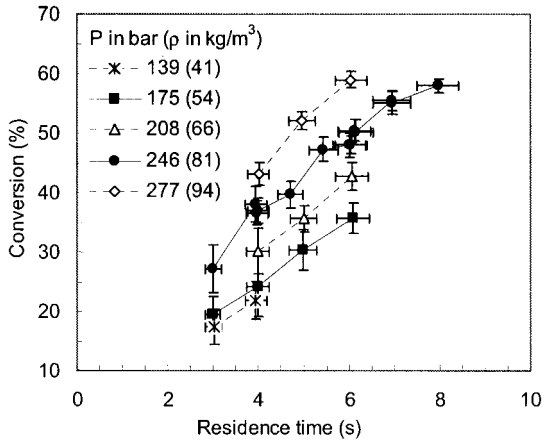

Figure 7. MPA conversion as a function of pressure (water density) and residence time. These data were measured at T = 528 ± 3°C, Φ = 1.01 ± 0.05, and $[MPA]_0$ = 1.00 ± 0.03 mM.

The 551°C data also showed a strong dependence of MPA conversion on the water density; for example, at τ=5 s, the conversion increased from 64±2% at ρ=51 kg/m^3 (P=173 bar) to 77±1% at ρ=76 kg/m^3 (P=246 bar). Although the carbon fractions are not shown for this data set, the results were similar to those shown for the Φ variation experiments in Figure 6. As the MPA conversion increased with increasing water density, the CO_2 carbon fraction increased substantially, while the CH_4 carbon fraction remained relatively constant. The CO carbon fraction did increase with increasing water density at the lower water densities where the MPA oxidation rates are slow; however, at higher densities and MPA conversions, the CO carbon fraction was approximately constant. Earlier studies of CO oxidation by our group indicated a marked dependence on water density or pressure (Holgate et al., 1994a). Due to the complex role that water plays as a three-body collider and a reactant in the free radical dominated networks, it is difficult to hypothesize exactly how water influences MPA oxidation in SCW. An elementary reaction rate model for MPA in SCW has been developed to provide further mechanistic insights (see, for example, Sullivan et al., 2004).

Dependence on initial MPA concentration

The final set of experiments was conducted at Φ=1.00±.06, P=246±1 bar, and T=528±3°C at $[MPA]_0$=0.5 and 1.0 mM to determine if MPA oxidation rates are dependent on the initial concentration, $[MPA]_0$. Due to the combination of solubility and detection limits, the MPA feed concentrations could only be studied over a limited range. Decreasing $[MPA]_0$ by 50% caused a minimal decrease in MPA conversion: at τ=3 s, the conversion decreased from 27±4 to 24±2%, at τ=4 s, the conversion decreased from 37±2 to 31±2%, and at τ=6.2 s the conversion decreased from 50±2 to 45±3%. These conversion values are approximately equal within experimental error bounds, indicating that MPA conversion is nearly independent of $[MPA]_0$.

A lack of dependence of MPA conversion on initial concentration is consistent with a first-order kinetic behavior. First-order rate constants were calculated from stoichiometric MPA oxidation data at different residence times to determine if they were constant at specified temperatures and pressures (P=246 bar). If MPA follows first-order behavior, then a plot of ln(1-conversion) = ln(1-X) vs τ, as shown in Figure 8, should be linear for each temperature with a slope equal to the first-order rate constant, -k

$$-\frac{d[\mathrm{MPA}]}{dt} = k[\mathrm{MPA}] \tag{4}$$

$$\ln\left(\frac{[\mathrm{MPA}]}{[\mathrm{MPA}]_0}\right) = \ln(1-X) = -k\tau \tag{5}$$

The linearity of the data set for each temperature shown in Figure 8 verifies first-order dependence, consistent with measured SCWO rates for other organic compounds, including methane and carbon monoxide (Webley and Tester, 1991; Holgate et al., 1992).

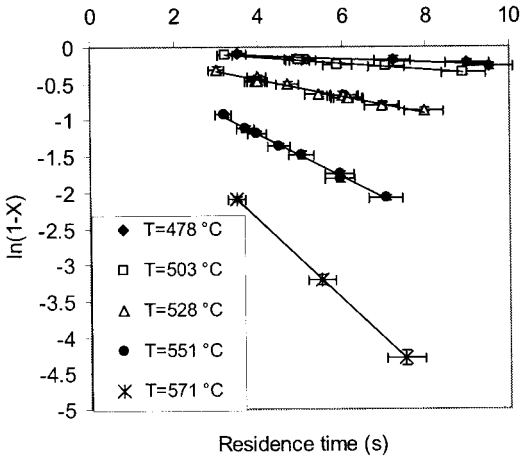

Figure 8. First-order plot of ln(1 − *X*) as a function of residence time for five different temperatures.

All of these data were taken at Φ = 0.98 ± 0.07, $[MPA]_0$ = 0.99 ± 0.03 mM, and P = 246 ± 1 bar. The slope at each temperature is equal to $-k$, the effective first-order rate constant.

Global rate law regression

An empirical global rate law for MPA oxidation was developed as a convenient means for correlating MPA conversion data as a function of T, [MPA], $[O_2]$, and $[H_2O]$

$$-R_{MPA} = -\frac{d[\mathrm{MPA}]}{dt} = A\exp\left(\frac{-E_a}{RT}\right)[\mathrm{MPA}]^a[\mathrm{O_2}]^b[\mathrm{H_2O}]^c \tag{6}$$

Here, A is the pre-exponential factor, E_a is the activation energy and a, b, and c are the reaction orders of MPA, O_2, and H_2O, respectively. Since the experimental data were measured at varying MPA, O_2, and H_2O concentrations, their effects could be quantitatively determined using multiple variable parameter regression. Plug-flow behavior in the reactor could be reasonably assumed since all experiments were in the turbulent flow region (Reynolds number >3000). The global rate law was regressed as using the plug-flow reactor design equation as

$$\frac{\tau}{[\mathrm{MPA}]_0} = \int_0^X \frac{dX}{-R_{MPA}} \tag{7}$$

In order to integrate Eq. 7, the overall rate, R_{MPA}, must be expressed in terms of MPA conversion. The water concentration was assumed to be constant and equal to the molar density of pure water at the T and P of each experiment since it is very large and does not change significantly during oxidation. The oxygen concentration was expressed in terms of MPA conversion as:

$$[\mathrm{O_2}] = [\mathrm{MPA}]_0\left(\frac{S}{\Phi} - SX\right) \tag{8}$$

where S is the stoichiometric ratio of O_2:MPA. If S is set to 2, this is equivalent to assuming complete oxidation of the carbon

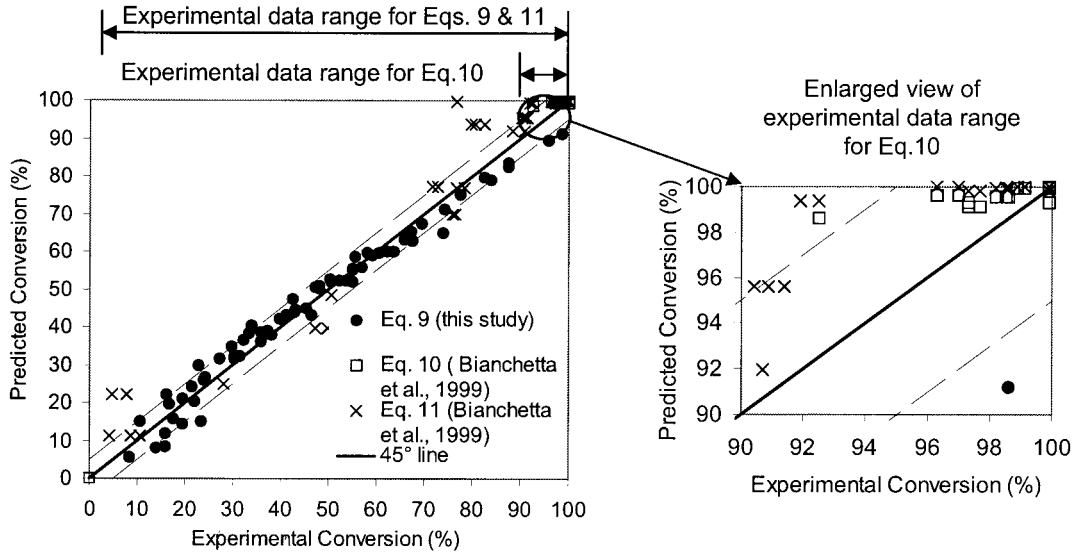

Figure 9. Predicted conversions compared to experimental conversions for the three global rate laws (Eqs. 9 to 11) using their respective data sets.

The data ranges for each equation are shown at the top of the figure. The dashed lines represent ±5% uncertainty in conversion predictions to demonstrate the accuracy of each global rate law.

in MPA to CO_2. However, at the conditions studied, MPA also reacts to the intermediates, CO and CH_4, which accumulate to finite values, thus causing S to be less than 2. By comparing measured O_2 and MPA conversions, a stoichiometric ratio of 1.3 would be more appropriate for the conditions studied. However, setting $S=1.3$ did not improve the regression predictions and did not change the fitted parameters outside the 95% confidence interval. Thus, we set $S=2$ for all global regressions as the carbon product distribution would not be known *a priori* to assign a best fit value of the stoichiometric ratio.

The nonlinear regression was calculated in MATLAB using the Marquardt method from a published algorithm (Constantinides and Mostoufi, 1999). For each data point in the program, the dependent variable was temperature, the independent variable was MPA conversion, and Φ, $[MPA]_0$, $[H_2O]$, and τ were input parameters. The 95% confidence intervals for each parameter were also calculated. In an effort to decrease the number of fit parameters, first-order dependence for MPA was assumed, that is, $a=1$, since the experimental data indicate such behavior based on the linear data in Figure 8. An attempt was also made to regress the reaction order of MPA and a value of $a=0.55\pm0.14$ was estimated. However, when the goodness of the overall fit of this rate law was compared with the expression with $a=1$, no significant difference was found. Thus, we chose to retain the value of $a=1$ for the global rate law based on the experimental evidence. The resulting global rate law is shown below with 95% confidence intervals for each parameter

$$\frac{-d[\mathrm{MPA}]}{dt} = 10^{14.0\pm1.6}\exp\left(\frac{-(228\pm22)\times10^3}{RT}\right) \times [\mathrm{MPA}][\mathrm{O_2}]^{0.30\pm0.18}[\mathrm{H_2O}]^{1.17\pm0.30} \quad (9)$$

The activation energy of $228\pm22\text{x}10^3$ is in J/mol and all concentrations are in mol/L. Consistent with experimental results, the MPA oxidation rate exhibits a dependence on MPA, O_2, and H_2O concentrations.

Bianchetta et al. (1999) also developed two global rate laws for MPA oxidation. The authors did not adjust the water concentration experimentally, so they did not include water concentration in their regression. Also, since the majority of the data were taken at 200% excess oxygen, the oxygen concentration was assumed constant in their rate law. The first global rate law regressed from 17 data points with conversions greater than 92% assumed first-order MPA dependence and predicted first-order O_2 dependence as shown in Eq. 10

$$\frac{-d[\mathrm{MPA}]}{dt} = 10^{14.09\pm9.11}\exp\left(\frac{-186\pm36}{RT}\right)[\mathrm{MPA}][\mathrm{O_2}]^{1.01\pm0.65} \quad (10)$$

The activation energy is kJ/mol and the concentrations are in mol/L. A second global rate law was developed from all 43 data points with an assumed first-order MPA dependence and 0.33 order O_2 dependence in Eq. 11

$$\frac{-d[\mathrm{MPA}]}{dt} = 10^{12.57\pm8.13}\exp\left(\frac{-186\pm36}{RT}\right)[\mathrm{MPA}][\mathrm{O_2}]^{0.33} \quad (11)$$

The first global rate law in Eq. 10 provides an accurate global rate law for high conversion conditions for more practical applications, while the rate law in Eq. 11 is a correlation of all of the data collected in their study, at both low and high conversions.

To determine how well each global rate law represents its corresponding data set, conversions were predicted by integrating Eqs. 9 to 11 and compared them to measured experimental conversions. In Figure 9, predicted conversions for the exper-

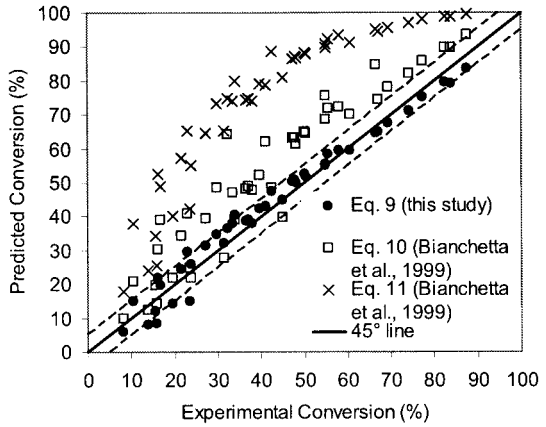

Figure 10. Predicted conversions compared to experimental conversions for the three different global rate laws (Eqs. 9 to 11) with the data from the present MPA experiments.

The dashed lines represent ±5% uncertainty in conversion predictions to demonstrate the accuracy of each global rate law.

imental data from this study are shown with a 45° line and ±5% conversion dotted lines to illustrate the accuracy of the predicted conversions. The predicted conversions for the Bianchetta et al data from the global rate laws in Eqs. 10 and 11 are also included for comparison. To better represent Bianchetta et al.'s high conversion data, a magnified plot for $X > 90\%$ was also included. For the present MPA study, the majority of the data are predicted within ±5% conversion by the regressed global rate law. As expected, the high and low conversion data predictions contain the largest uncertainty. Predicted conversions from Eqs. 10 and 11 also agree reasonably well with their corresponding data sets.

Given the three global rate laws in Eqs. 9 to 11, we wanted to determine how well each expression predicts the present MPA oxidation data. The integration of each equation was performed with their limiting assumptions, that is, constant $[O_2]$ was assumed for the integration of Eqs. 10 and 11, and the calculated results are presented in Figure 10. The global rate law from Eq. 9 agrees with the experimental results satisfactorily while the other two global rate laws predict substantially higher conversions. The predicted rate constants from Eq. 11 are almost twice as large as those from Eq. 10 because of the different oxygen orders in the two equations. The limiting assumption of constant excess oxygen leads to an effective pre-exponential factor of $A^*[O_2]_0^b$ equal to $10^{14.09\pm9.11}[O_2]_0^{1.01\pm0.65}$ in Eq. 10 and $10^{12.57\pm8.13}[O_2]_0^{0.3}$ in Eq. 11. At the average oxygen concentrations examined in the present study ($[O_2]_0 \approx 2$ mM), the effective pre-exponential factor almost doubles from $2.5\text{x}10^{11}$ for Eq. 10 to $4.8\text{x}10^{11}$ for Eq. 11. However, for the Bianchetta et al. data, $[O_2]_0 \approx 4$ mM, increasing the effective pre-exponential factor slightly from $4.9\text{x}10^{11}$ to $6.0\text{x}10^{11}$ for the two equations. This indicates that the global rate laws in Eqs. 10 and 11 may not be appropriate for lower oxygen concentrations ($\Phi > 1$) since they were developed with the limiting assumption of constant excess oxygen concentration conditions ($\Phi < 0.5$).

Macroscopic pathways analysis

To estimate the relative reaction rates of the major carbon pathways in MPA oxidation, a model was developed using the four pathway mechanism as hypothesized in Figure 5. The relevant set of ordinary differential equations for this model is given by

$$\frac{d[\text{MPA}]}{dt} = -k_1[\text{MPA}][O_2]^{b_1} - k_2[\text{MPA}][O_2]^{b_2} \quad (12)$$

$$\frac{d[\text{CO}]}{dt} = k_1[\text{MPA}][O_2]^{b_1} + k_4[CH_4][O_2]^{b_4} - k_3[\text{CO}][O_2]^{b_3} \quad (13)$$

$$\frac{d[CH_4]}{dt} = k_2[\text{MPA}][O_2]^{b_2} - k_4[CH_4][O_2]^{b_4} \quad (14)$$

$$\frac{d[CO_2]}{dt} = k_3[\text{CO}][O_2]^{b_3} \quad (15)$$

$$\frac{d[O_2]}{dt} = -k_1[\text{MPA}][O_2]^{b_1} - k_2[\text{MPA}][O_2]^{b_2} - k_3[\text{CO}][O_2]^{b_3} - k_4[CH_4][O_2]^{b_4} \quad (16)$$

$$k_i = A_i \exp\left(\frac{-E_{a,i}}{RT}\right) \quad \text{for } i = 1, \ldots, 4 \quad (17)$$

Using these equations, the parameters, A_i, $E_{a,i}$, and b_i were regressed for each reaction pathway in MATLAB using the Marquardt algorithm and the MATLAB function, "ode23", to solve the differential equations (Constantinides and Mostoufi, 1999). All pathways were assumed to follow first-order behavior with respect to MPA, CO, and CH_4 since the global rate laws for each of these compounds also predict first-order behavior (Holgate et al., 1992; Webley and Tester, 1991). Carbon monoxide can react by two different pathways in supercritical water: the water-gas shift reaction and direct CO oxidation. Given the high O_2:CO concentration ratios and the higher temperatures during MPA oxidation, the CO reaction would primarily occur through the oxidation pathway; as such, the water-gas shift pathway was not included in the MPA oxidation model. The water density variation data were excluded from the regression since an explicit dependence on water is not included in these rate constants. All data used in these regressions were at a constant pressure of 246 bar, in a water concentration range from 4.1 to 5.2 M or a density range of 73 to 93 kg/m^3.

The macroscopic reaction rates are shown in Table 2, which also includes parameters from the pure CO and CH_4 oxidation rates in the literature for comparison (Webley and Tester, 1991; Holgate et al., 1992). Pseudo-first-order rate constants are included as a means of comparison between the different reaction rates. For these rate constants, $[O_2]$ is assumed to be constant at 2 mM, the initial concentration of O_2 in most of the MPA experiments.

The regressed reaction rate for CH_4 reaction to CO, k_4, is not

Table 2. Reaction Rate Parameters for the Macroscopic Reaction Rates in MPA Oxidation Based on the Model of Eqs. 12 to 16 with First-Order Dependence*

Parameter	$\left(\frac{d[\text{MPA}]}{dt}\right)_{i=1}$	$\left(\frac{d[\text{MPA}]}{dt}\right)_{i=2}$	$\left(\frac{d[\text{CO}]}{dt}\right)_{i=3}$	$\left(\frac{d[\text{CO}]}{dt}\right)_{lit,i=3}$	$\left(\frac{d[\text{CH}_4]}{dt}\right)_{lit,i=4}$
$\log_{10}(A)$	11.3 ± 0.1	12.5 ± 0.5	9.8 ± 0.2	8.5 ± 3.3	11.4 ± 1.1
E_a (kJ/mol)	176 ± 2	218 ± 10	146 ± 3	134 ± 32	179 ± 18
b_i for O_2	0.28 ± .05	0.03 ± .03	0.31 ± .06	0.34 ± 0.24	0.66 ± 0.14
T (°C)	k_1 $(M^{0.28}s)^{-1}$	k_2 (s^{-1})	k_3 $(M^{0.31}s)^{-1}$	k_3(lit) $(M^{0.34}s)^{-1}$	$k_4(lit)$ $(M^{0.66}s)^{-1}$
478	1.9E-02	2.0E-03	6.1E-02	1.8E-02	1.5E-03
503	4.8E-02	6.1E-03	1.3E-01	3.7E-02	3.7E-03
528	1.1E-01	1.8E-02	2.6E-01	7.0E-02	8.9E-03
551	2.3E-01	4.4E-02	4.8E-01	1.2E-01	1.9E-02
571	4.3E-01	9.3E-02	8.0E-01	1.9E-01	3.5E-02

*The subscripts for the MPA and CO rates refer to the pathway components shown in Figure 5. Global rates for CO and CH_4 oxidation from literature values, specifically k_3 from Eq. 22 in Holgate et al. (1992) and k_4 from Eq. 4 in Webley et al. (1991) are also included, along with pseudo first-order rate constants, assuming $[O_2]_0 = 2$ mM, for each reaction rate.

included in Table 2 because the reaction rate for CH_4 to CO oxidation was estimated not to be statistically different than zero from the regression results. Since the CH_4 concentration in the system is very low, it was difficult to estimate both the CH_4 production (k_2) and oxidation (k_4) rates with any confidence. The CH_4 oxidation rate from Webley and Tester (1991) is slower than the rate of CH_4 production (k_2) at all temperatures, leading to CH_4 accumulation during MPA oxidation. The formation reaction rate expression for CH_4 is independent of O_2 concentration with $b_2=0.03\pm0.03$ or $b_2\approx 0$, because the reaction pathway from MPA to CH_4 occurs by reduction, not oxidation.

The CO oxidation rate constant to form CO_2, k_3, is compared to an experimental value determined earlier in Holgate et al. (1992) (see Table 2). The estimated value for k_3 from the MPA regression is approximately three to four times larger than the rate constant from the earlier pure CO experiments. An initial attempt was made to include the CO literature parameters in the regression of Eqs. 12 to 17; however, this CO oxidation rate was too slow at all conditions so the CO oxidation rate, k_3, was regressed from the MPA oxidation data. The CO oxidation rates could be faster during MPA oxidation than for pure CO oxidation due to co-oxidation effects (Savage et al., 2000 and Webley et al., 1991). CO oxidation to CO_2 is primarily dependent on the OH radical. If the OH radical concentration is higher during pure MPA oxidation than for CO oxidation, CO would react faster in the MPA system.

The MPA oxidation rates, k_1 and k_2, are also estimated in Table 2. The branching between the two MPA pathways is the ratio of k_1:k_2, which decreases from 10 at $T=478$°C to 5 at $T=571$°C. This indicates that the second, slower pathway to CH_4 becomes more significant as the temperature increases. Experimentally, the methane yield increased from 0.05 at $T=503$°C to 0.19 at $T=571$°C in Figure 3 showing that the methane pathway does become more important at higher temperatures. However, k_1, the oxidation rate for MPA to CO formation remains the dominant reaction rate at all temperatures.

Finally, we return to the experimental observation that k_1, the reaction rate of MPA to CO, and k_3, the reaction rate of CO to CO_2, have similar time scales leading to accumulation of the CO intermediate at lower temperatures. These two rates, k_1 and k_3, shown in Table 2 are within a factor of about 2 of each other, indicating that oxidation of MPA and CO are indeed occurring at comparable rates. Also, the oxygen orders of both reactions were estimated in Table 2 to be about 0.3, the same as the O_2 order in the MPA global rate laws in Eqs. 9 and 11, and in the CO global rate law from literature (Holgate et al., 1992). From the independence of CO carbon fraction on O_2 concentration, similar oxygen orders for k_1 and k_3 would be expected. However, it is difficult to speculate on what a global O_2 order of 0.3 implies mechanistically. A full elementary reaction rate model has been developed to quantify this effect (see Sullivan et al., 2004).

Conclusions

An experimental study of MPA hydrolysis and oxidation in SCW was completed that systematically explored the effects of temperature, residence time, oxygen concentration, MPA concentration, and pressure (or water density) on MPA conversion and on its product distribution. Conversion due to hydrolysis was less than 6% after $\tau=7$ s at all temperatures studied. Minimal conversion ($X<30\%$ at $\tau=10$ s) was measured at $T<503$°C, while almost complete conversion ($X=99\%$) was measured at $T=571$°C and $\tau=7$ s at stoichiometric conditions and $P=246$ bar. MPA oxidation rates exhibited a dependence on both oxygen concentration and pressure (or water density), but were relatively independent of initial MPA concentration. A global rate law was also developed with a first-order dependence on MPA and a non-zero dependence on both oxygen and water concentrations.

MPA oxidation occurs by two pathways to the carbon-containing intermediates, CO and CH_4. The dominant pathway is through the CO intermediate to the final carbon-containing product, CO_2. A macroscopic model was developed to estimate the relative reaction rates of these major pathways in MPA oxidation. The branching ratio of CO to CH_4 production was approximately 5 to 10, decreasing as temperature increased. The reaction rate constants for oxidation of MPA to CO, k_1, and CO to CO_2, k_3, were of the same order of magnitude indicating that these rates occur on similar time scales. For the CO and CH_4 intermediates, CH_4 was unreactive during MPA oxidation while CO oxidation occurred more quickly during MPA oxidation than during pure CO oxidation due to co-oxidation effects.

Acknowledgements

The authors would like to acknowledge support from the Army Research Office through the University Research Office under the guidance of Dr. Robert Shaw (Grant No. DAAD 19-99-1-0211) and from a National Science Foundation Graduate Research Fellowship. We would also like to thank Professors K.C. Swallow, Bill Green, Jack Howard, Ken Smith, and Dr. Bill Peters for helpful discussions and advice in this work. In addition, this work would not have been possible without the assistance and helpful discussions with past and present members of the MIT SCWO research group, including Russell Lachance, Jason Ploeger, Michael Timko, Dr. Joshua Taylor, and Dr. Joanna Blanchard-DiNaro.

Literature Cited

ACWA, *Assembled Chemical Weapons Assessment Program-Supplemental Report to Congress,* (1999).

Bianchetta, S., L. Li and E. F. Gloyna, "Supercritical Water Oxidation of Methylphosphonic Acid," *Ind. Eng. Chem. Res.,* **38**, 2902 (1999).

Constantinides, A. and N. Mostoufi, *Numerical Methods for Chemical Engineers with Matlab Applications*, Prentice Hall PTR, Upper Saddle River, NJ (1999).

Cordeiro, J. L., D. L. Pompliano and J. W. Frost, "Degradation and Detoxification of Organophosphonates: Cleavage of the Carbon to Phosphorus Bond," *J. Am. Chem. Soc.,* **108**, 332 (1986).

DiNaro, J. L., "Oxidation of Benzene in Supercritical Water: Experimental Measurements and Development of an Elementary Reaction Mechanism," PhD Thesis, Dept. of Chemical Engineering, Massachusetts Institute of Technology, Cambridge, MA (1999).

DiNaro, J. L, J. W. Tester, J. B. Howard and K. C. Swallow, "Experimental Measurements of Benzene Oxidation in Supercritical Water," *AIChE J.,* **46**(11), 2274 (2000a).

DiNaro, J., J. Howard, W. Green, J. W. Tester and J. Bozzelli, "Elementary Reaction Mechanism for Benzene Oxidation in Supercritical Water," *J. Phys. Chem. A,* **104**(45), 10576 (2000b).

Glaude, P. A., H. J. Curran, W. J. Pitz and C. K. Westbrook, "Kinetic Study of the Combustion of Organophosphorus Compounds," *Proc. of the Combustion Institute,* **28**, 1749 (2000).

Gloyna, E. F. and L. Li, "Supercritical Water Oxidation Research and Development Update," *Environ. Prog.,* **14**(3), 182 (1995).

Helling, R. K., and J. W. Tester, "Oxidation Kinetics of Carbon Monoxide in Supercritical Water," *Energy Fuels,* **1**, 417 (1987).

Holgate, H. R., P. A. Webley, J. W. Tester, and R. K. Helling, "Carbon Monoxide Oxidation in Supercritical Water: The Effects of Heat Transfer and The Water-Gas Shift Reaction on Observed Kinetics," *Energy Fuels,* **6**(5), 586 (1992).

Holgate, H. R., and J. W. Tester, "Oxidation of Hydrogen and Carbon Monoxide in Sub- and Supercritical Water: Reaction Kinetics, Pathways, and Water-Density Effects. 1. Experimental Results," *J. Phys. Chem.,* **98**, 800 (1994a).

Holgate, H. R., and J. W. Tester, "Oxidation of Hydrogen and Carbon Monoxide in Sub- and Supercritical Water: Reaction Kinetics, Pathways, and Water-Density Effects. 2. Elementary Reaction Rate Modeling," *J. Phys. Chem.,* **98**(3), 810 (1994b).

Koo, M., W. K. Lee, and C. H. Lee, "New Reactor System for Supercritical Water Oxidation and its Application on Phenol Destruction," *Chem. Eng. Sci.,* **52**(7), 1201 (1997).

Korobeinichev, O. P., S. B. Ilyin, T. A. Boshova, V. M. Shvartsberg, and A. A. Chernov, "The Chemistry of the Destruction of Organophosphorus Compounds in Flames -III: The Destruction of DMMP and TMP in a Flame of Hydrogen and Oxygen," *Combustion and Flame,* **121**, 593 (2000).

Kritzer, P., and E. Dinjus, "An Assessment of Supercritical Water Oxidation (SCWO) - Existing Problems, Possible Solutions and New Reactor Concepts," *Chem. Eng. J.,* **83**(3), 207 (2001).

Modell, M., "Supercritical Water Oxidation," *Standard Handbook of Hazardous Waste Treatment and Disposal*, H. M. Freeman, ed., McGraw Hill, New York, pp. 8.153-8.168 (1989).

NRC, *Integrated Design of Alternative Technologies for Bulk-Only Chemical Agent Disposal Facilities,* National Academy Press, Washington DC (2000).

Phenix, B., J. Dinaro, J. Tester, J. Howard, and K. Smith, "The Effects of Mixing and Oxidant Choice on Laboratory-Scale Measurements of Supercritical Water Oxidation Kinetics," *Ind. Eng. Chem. Res.,* **41**(3), 624 (2002).

Savage, P. E., S. Gopalan, T. I. Mizan, C. J. Martino, and E. E. Brock, "Reactions at Supercritical Conditions: Applications and Fundamentals," *AIChE J.,* **41**(7), 1723 (1995).

Savage, P., J. Yu, N. Stylski, and E. Brock, "Kinetics and Mechanism of Methane Oxidation in Supercritical Water," *J. Supercrit. Fluids,* **12**, 141 (1998).

Savage, P. E., "Organic Chemical Reactions in Supercritical Water," *Chem. Rev.,* **99**(2), 603 (1999).

Savage, P., J. Rovira, N. Stylski, and C. Martino, "Oxidation Kinetics for Methane/Methanol Mixtures in Supercritical Water," *J. Supercrit Fluids,* **17**, 155 (2000).

Schowanek, D., and W. Verstraete, "Hydrolysis and Free Radical Mediated Degradation of Phosphonates," *J. Environ Quality,* **20**, 769 (1991).

Shaw, R. W., and N. Dahmen, "Destruction of Toxic Organic Materials Using Supercritical Water Oxidation: Current State of the Technology," *Supercritical Fluids*, E. Kiran et al., eds., Kluwer Academic Publishers, Netherlands (2000).

Sullivan, P.A. "Oxidation Kinetics of Methylphosphonic Acid in Supercritical Water: Experimental Measurements and Model Development," PhD Thesis, Dept. of Chemical Engineering, Massachusetts Institute of Technology, Cambridge, MA (2003).

Sullivan, P.A., J.W. Tester, et al., "Elementary Reaction Mechanism for Methylphosphonic Acid Oxidation in Supercritical Water" submitted to *Phys. Chem. Chem. Phys.* (2004).

Tester, J. W., H. R. Holgate, F. J. Armellini, P. A. Webley, W. R. Killilea, G. T. Hong, and H. E. Barner, "Supercritical Water Oxidation Technology: A Review of Process Development and Fundamental Research," *Emerging Technologies in Hazardous Waste Managemen,* Vol. III, Chap. 3, D. W. Tedder and F. G. Pohland, eds., ACS Symp. Ser., Vol. 518 (1993).

Tester, J. W. and J. A. Cline, "Hydrolysis and Oxidation in Sub- and Supercritical Water: Connecting Process Engineering Science to Molecular Interactions," *Corrosion,* **55**, 1088 (1999).

Turner, M. D., "Supercritical Water Oxidation of Dimethyl Methylphosphonate and Thiodiglycol," PhD Thesis, Dept. of University of Texas at Austin, Austin, TX (1993).

Webley, P. A., and J. W. Tester, "Fundamental Kinetics of Methane Oxidation in Supercritical Water," *Energy Fuels,* **5**, 411 (1991).

Webley, P. A., J. W. Tester, and H. R. Holgate, "Oxidation Kinetics of Ammonia and Ammonia-Methanol Mixtures in Supercritical Water in the Temperature Range 530-700°C at 246 bar," *Ind. Eng. Chem. Res.,* **30**(8), 1745 (1991).

Werner, J. H., and T. A. Cool, "Kinetic Model for the Decomposition of DMMP in a Hydrogen/Oxygen Flame," *Combustion and Flame,* **117**, 78 (1998).

Zegers, E. J., and E. M. Fisher, "Gas-phase Pyrolysis of Diethyl Methylphosphonate," *Combust. Sci. Technol.* **116**(1-6) 69 (1996).

Zegers, E. J. P., and E. M. Fisher, "Gas-Phase Pyrolysis of Diisopropyl Methylphosphonate," *Combust. Flame,* **115**(1-2), 230 (1998).

Manuscript received Jun. 26, 2003, and final revision received Sept. 3, 2003.